Journal of Biomechanics 163 (2024) 111913

Contents lists available at ScienceDirect

Journal of Biomechanics

journal homepage: www.elsevier.com/locate/jbiomech

In vivo strain measurements in the human buttock during sitting using MR-based digital volume correlation

Stefano Zappalá [a,b,*], Bethany E. Keenan [c], David Marshall [a], Jing Wu [a], Sam L. Evans [c], Rami M.A. Al-Dirini [d]

[a] School of Computer Science and Informatics, Cardiff University, Cardiff, UK
[b] Cardiff University Brain Research Imaging Centre (CUBRIC), School of Psychology, Cardiff University, Cardiff, UK
[c] School of Engineering, Cardiff University, Cardiff, UK
[d] College of Science and Engineering, Flinders University of South Australia, Adelaide, Australia

ARTICLE INFO

Dataset link: https://tinyurl.com/36x2npyt

Keywords:
Digital volume correlation
Strain analysis
Deep tissue injury
Pressure ulcers
Soft tissues

ABSTRACT

Advancements in systems for prevention and management of pressure ulcers require a more detailed understanding of the complex response of soft tissues to compressive loads. This study aimed at quantifying the progressive deformation of the buttock based on 3D measurements of soft tissue displacements from MR scans of 10 healthy subjects in a semi-recumbent position. Measurements were obtained using digital volume correlation (DVC) and released as a public dataset. A first parametric optimisation of the global registration step aimed at aligning skeletal elements showed acceptable values of Dice coefficient (around 80%). A second parametric optimisation on the deformable registration method showed errors of 0.99 mm and 1.78 mm against two simulated fields with magnitude 7.30 ± 3.15 mm and 19.37 ± 9.58 mm, respectively, generated with a finite element model of the buttock under sitting loads. Measurements allowed the quantification of the slide of the gluteus maximus away from the ischial tuberosity (IT, average 13.74 mm) that was only qualitatively identified in the literature, highlighting the importance of the ischial bursa in allowing sliding. Spatial evolution of the maximus shear strain on a path from the IT to the seating interface showed a peak of compression in the fat, close to the interface with the muscle. Obtained peak values were above the proposed damage threshold in the literature. Results in the study showed the complexity of the deformation of the soft tissues in the buttock and the need for further investigations aimed at isolating factors such as tissue geometry, duration and extent of load, sitting posture and tissue properties.

1. Introduction

A pressure ulcer is localised damage to the skin and/or underlying tissues over bony prominences, often due to prolonged compression and shear strains induced by contact with support surfaces (Sonenblum et al., 2020; Gefen, 2008; Zeevi et al., 2018; Brienza et al., 2018; Bartley and Stephens, 2019). Despite preventative measures, pressure ulcers remain a burden on healthcare systems. In the UK, up to 202,000 people developed annually a new pressure ulcer in the period 2017/18, leading to an average annual cost of £748 for healed and £5972 for unhealed wounds per patient (Guest et al., 2020). The highest incidence of pressure ulcers was observed in the sacrum and buttocks across six hospitals in the UK (Fletcher et al., 2013).

Deep tissue injury (DTI) is a pressure ulcer that originates at internal tissues surrounding bony prominences such as the ischial tuberosity (IT), greater trochanter (GT) and the sacrum (Zeevi et al., 2018; Schwartz and Gefen, 2019). DTIs can, sometimes, be initially miscategorised or even diagnosed as late as 24–72 h after the initial onset (Black et al., 2016). This is partly because DTIs are not always associated with broken skin or an open wound (Fletcher et al., 2017). Age, impaired mobility, continence, temperature and nutrition are all factors that can contribute to the onset of DTI (Linder-Ganz et al., 2007; Westby et al., 2017; Oomens et al., 2003). However, the relatively large mechanical deformation of soft tissue seems to be the dominant initiating factor (Linder-Ganz et al., 2007; Bouten et al., 2003; Nelissen et al., 2018).

In vivo deformation of deep soft tissues can be measured, non-invasively, using magnetic resonance (MR) imaging (Makhsous et al., 2011; Al-Dirini et al., 2017; Linder-Ganz et al., 2007; Sonenblum et al., 2015). Previous measurements largely assumed a 2D behaviour of soft tissue deformation (Al-Dirini et al., 2015; Makhsous et al.,

* Correspondence to: CUBRIC, Maindy Road, Cardiff, CF24 4HQ, UK.
E-mail address: zappalas@cardiff.ac.uk (S. Zappalá).

https://doi.org/10.1016/j.jbiomech.2023.111913
Accepted 20 December 2023
Available online 22 December 2023

2011; Sonenblum et al., 2013; Shabshin et al., 2010). However, there is growing evidence that soft tissues in the human buttock undergo complex, 3D deformation under sitting loads (Sonenblum et al., 2015; Al-Dirini et al., 2015, 2017; Linder-Ganz et al., 2008; Chen et al., 2020). In particular, the gluteus maximus was qualitatively observed to laterally shift away from the IT in sitting individuals, sometimes leaving little or no muscle to withstand the load (Sonenblum et al., 2020; Doridam et al., 2018; Wang et al., 2022). Yet, quantification of the full, 3D deformation field remains absent in the literature. Volumetric measurements of soft tissue deformation under physiological loads would progress understanding of the aetiology of DTI (Avril et al., 2013; Al-Dirini et al., 2016; Macron et al., 2020; Shabshin et al., 2010).

The aim of this study was to measure the 3D, progressive soft tissue deformation of the buttock under sitting loads. The deformation was quantified using digital volume correlation (DVC) of unloaded to loaded scans of the buttock for seated individuals. We hypothesised that soft tissue deformation during sitting is complex, 3D and highly variable between subjects. This study is based on the same dataset from Al-Dirini et al. (2017), but instead of capturing tissue deformation as 1D measurements of tissue thickness, it was determined as full field, 3D displacement map. To achieve that, global and deformable registration steps were carried out using three registration methods for medical imaging that are widely used in academia. Error analysis was carried out to gauge the margin of error associated with the DVC calculations and hence the confidence on the obtained results.

2. Methods

2.1. MR dataset

As part of a previous study (Al-Dirini et al., 2017), MR scans depicting the quasi-static deformation of gluteal soft tissues of ten healthy male subjects (aged 19–39, BMI = 28.02 ± 4.71 kg/m^2) were acquired. Each subject had 3D MR scans while in a semi-recumbent sitting posture, where each of the scans represented part of the progressive, quasi-static deformation of the pelvic soft tissues under sitting loads (Fig. 1a). First, a fully deformed condition was simulated by having both buttocks supported by wooden blocks (full-weight bearing (WB)). Second, a partially deformed condition was simulated by removing one of three 10 mm-thick wooden inserts that were placed under the left buttock (partial-WB). Finally, an undeformed state was simulated by removing all three blocks from the left side, leaving the right side to support the full weight of each subject (non-WB). Each volume represented the deformation at equilibrium for each simulated stage, as scanning was initiated only after between 5 to 6 min from the application of the load. A 1.5 T scanner was used to obtain proton-density weighted spin echo scans (TR = 4542 ms, TE = 32.18 ms) with an anisotropic resolution of $0.78 \times 0.78 \times 10$ mm^3 over a field of view of $401 \times 400 \times 481$ mm^3. Further details can be found in Al-Dirini et al. (2017).

A single observer used Simpleware ScanIP software (Simpleware ScanIP O-2018.12, Synopsys, Inc., Mountain View California, USA) to manually segment the gluteus maximus and subcutaneous fat, regions of interest (ROIs) of the study (Fig. 1b). Moreover, the following skeletal elements of the pelvis were outlined for the initial alignment of the scans: the femoral head, the left greater trochanter (GT), the left and right inferior pubic rami and the left IT (Fig. 2). The scanner-default correction for MR distortions was applied at the time of scanning. Given the coarse voxel spacing of the images along the inferior-superior direction (z-resolution = 10 mm), image deconvolution via software NiftyMIC (Ebner et al., 2020) was used to decrease the voxel spacing along the same direction. Optimal resolution for accurate DVC measurements was investigated in the optimisation step (details later on).

2.2. Digital volume correlation

Digital volume correlation was carried out by first running a global[1], intensity-based registration call to align pelvic bones to a common reference space, followed by deformable intensity-based registration (Schnaudigel et al., 2010; Zappalá et al., 2021; Monea et al., 2012) to capture the displacement field.

Global registration was essential for the proper initialisation of the deformable registration. It was restricted to the segmented pelvic bones, which could be considered as rigid references for the deformation during the MR experiment. This initial alignment of skeletal elements also corrected for the rigid body motion reported by Al-Dirini et al. (2017), as subjects in the dataset could not maintain the exact same posture for all three scans (change in pelvic tilt <6°). The full-WB scan of each participant was chosen as subject reference and all other scans were registered to that space, as it presented a consistent posture with both buttocks supported during scanning.

The progressive deformation of the soft tissues was obtained by two stages of deformable registration (Fig. 1c). First, the bone-aligned non-WB scan of each subject was morphed to the corresponding partial-WB scan. This will be referred to as the 1st stage of deformation. Then, the bone-aligned partial-WB scan was morphed to the corresponding full-WB scan, which will be referred to as 2nd stage of deformation (Fig. 1c).

DVC error analysis. A first comparative analysis was performed to assess the error associated with the global registration of skeletal elements. Three global methods for medical image registration that are widely used in academia were optimised and compared: FLIRT (from the FSL suite) (Jenkinson et al., 2002), ANTs (Avants et al., 2008) and *elastix* (Klein et al., 2010). These methods consist in the deformation of a moving volume onto a fixed one via some transformation model. The best alignment is achieved by maximising a similarity measure between corresponding neighbourhoods of the two volumes (Oliveira and Tavares, 2014; Sotiras et al., 2013). Methods were optimised against the same task consisting of the alignment of the skeletal elements previously introduced. Optimal parameter set was identified in terms of transformation model, similarity measure, number of samples compared at each iteration, size of similarity window, and z-resolution after deconvolution. This was performed on three subjects that spanned the range of BMI within the study cohort. Further details are given in the Supplementary Materials.

The most robust method was *elastix*, partly thanks to the random sampling that allowed larger similarly windows: 405 calls reached an acceptable Dice coefficient (Dice, 1945) of at least 0.80 (Avants et al., 2008; Xu et al., 2016) (against the 342 calls of FLIRT and 361 of ANTs). The optimal set was chosen as: affine transformation; advanced mattes mutual information; 1937 samples, 49 mm window's side length; 10 mm inferior-superior resolution.

A second comparative analysis was performed to identify the most suitable deformable registration method for the DVC measurements. Three deformable methods for medical image registration widely used in academia were optimised and compared (DRAMMS Ou et al., 2011, SyN Avants et al., 2009 and *elastix* Klein and Staring, 2011). The following parameters were optimised: B-spline knot spacing, spline order, size of compared regions, number of samples in each iteration, z-resolution after deconvolution, and intensity interpolation after initial global registration. The same cross-correlation was chosen as similarity measure for all methods, given the mono-modality quality of the registration problem. Moreover, a B-spline transformation model was selected to avoid those components of bias that would be introduced from adopting any physical-based deformation models in the registration calls. Optimal performance was determined against two artificial displacement

[1] Here global is used in reference to the deformation model, in that it is not spatially varying (Sotiras et al., 2013).

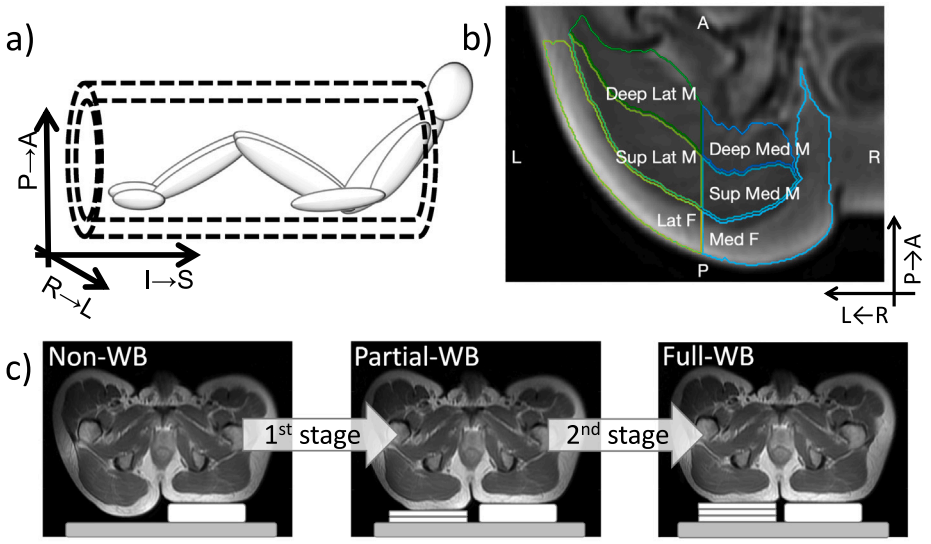

Fig. 1. Illustration of the acquisition set-up and reference system used (Al-Dirini et al., 2017). (a) Schematic representation of the positioning of the subject in the bore of the scanner relative to the chosen reference system: right–left (R→L), posterior-anterior (P→A) and inferior-superior (I→S). (b) Axial slice with the delineated regions of interest (ROIs): Deep Medial Muscle, Deep Lateral Muscle, Superficial Lateral Muscle, Superficial Medial Muscle, Lateral Fat, Medial Fat. (c) Depiction of the analysis of deformation carried out: 1st stage of deformation is here depicted as the transition from non-WB to partial-WB conditions and 2nd stage as the transition from partial-WB to full-WB conditions.

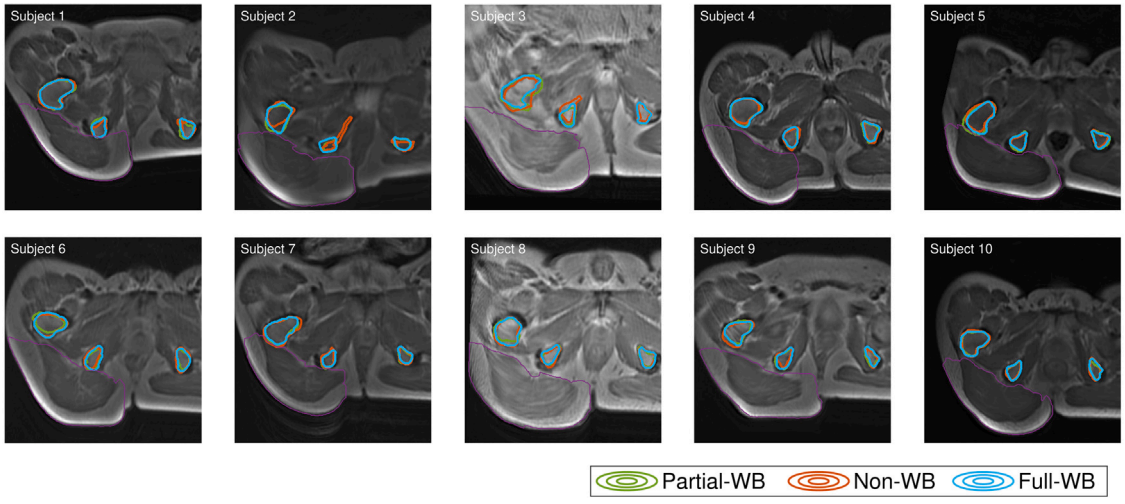

Fig. 2. Axial slices showing the initial alignment of the pelvic bones, here showing the IT. Masks of the skeletal elements for the full-WB condition are delineated in blue, in green for the partial-WB and in orange for the non-WB scans. In purple, the fat and muscle areas are delineated as reference. (For interpretation of the references to colour in this figure legend, the reader is referred to the web version of this article.)

fields emulating the large deformations of the buttock under sitting loads. These were generated with a simplified finite element (FE) model based on the non-WB anatomy of the subject with average BMI in the dataset (FEBio Suite Maas et al., 2012). Two loads with prescribed displacements of 10 mm and 30 mm were applied, simulating the transition from partial-WB to full-WB conditions (displacement: 7.30 ± 3.15 mm) as well as the larger non-WB to partial-WB transition (19.37 ± 9.58 mm). Neo-Hookean constitutive model was chosen for both the fat and muscle layers, with a Poisson's ratio of 0.49 and equivalent Young moduli of 30 kPa and 100 kPa, respectively (Bucki et al., 2019). Given the little influence of individual anatomies on the accuracy of the registration method tested by Schnabel et al. (2003), the obtained simulated fields were applied to the undeformed image of a single subject, ultimately reducing the number of registration calls (further details in the Supplementary Materials).

Again, *elastix* was found to be the best performing method and was used for the DVC measurements. However, given the large differences in the simulated fields, two parameter sets were identified specifically for the 1st stage of deformation (from the 10 mm simulation) and for the 2nd (from the 30 mm field) one. These were, respectively: 17 mm and 20 mm in-plane B-spline spacing, while 3 mm and 20 mm I→S spacing; 3 and 3 B-spline order; 82 mm and 58 mm size of compared regions; 3400 and 3600 samples at each iteration; 3 mm and 4 mm z-resolution; B-spline and sinc interpolations after initial registration. Errors associated to the optimal sets were 0.989 ± 0.943 mm against the 10 mm field, whereas 1.777 ± 1.854 mm against the 30 mm field (against 1.3879 ± 1.6271 mm and 1.8019 ± 2.1093 mm for DRAMMS and 1.2391 ± 1.6074 mm and 6.7968 ± 7.8748 mm for SyN, respectively — see Supplementary Materials).

Analysis of deformation. Analysis aimed at quantifying the differences in the deformation between the two stages of deformation both in the fat and muscle. These areas were split into medial and lateral sub-regions, and the latter further split into deep and superficial regions (Fig. 1b). Statistics were evaluated using MATLAB R2022b (Mathworks, Natick, MA, USA).

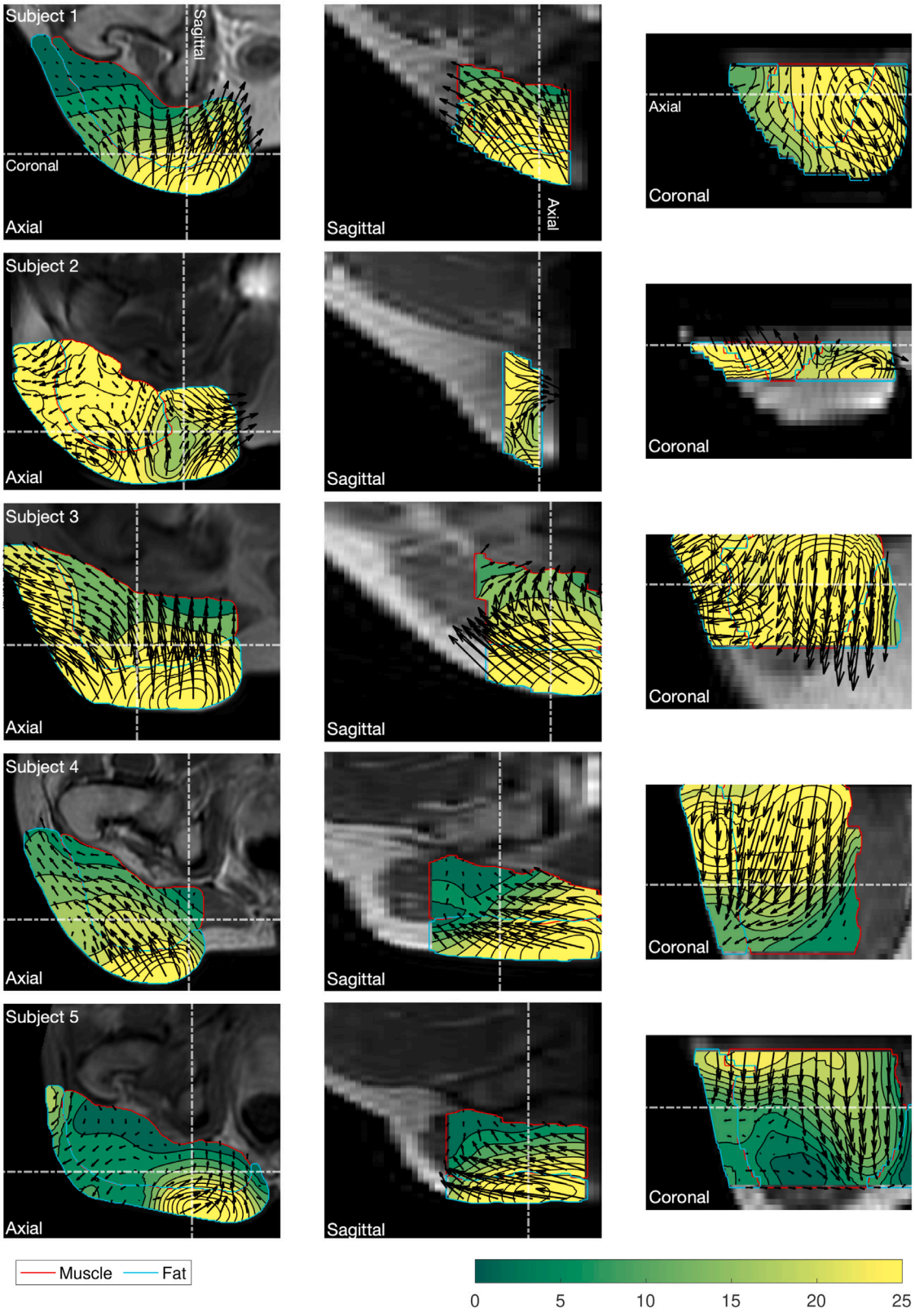

Fig. 3. Axial (left), sagittal (centre) and coronal (right) views of the displacement field for the first 5 subjects. Arrows show the direction of displacement vectors for the overall deformation (non-WB to full-WB). Length of vectors is scaled for visualisation purposes: magnitude is represented by the underlying colourmap (in [mm]). Muscle and fat ROIs are delineated in red and turquoise, respectively. Slices are located at the centre of the IT: dashed lines show the location of the other slices. (For interpretation of the references to colour in this figure legend, the reader is referred to the web version of this article.)

To further investigate the local state of deformation of the tissues, the distribution of the Green–Lagrange strain tensor, **E**, was extracted. This was defined as (Holzapfel, 2002):

$$\mathbf{E} = \frac{1}{2}\left(\mathbf{F}^T\mathbf{F} - I\right), \quad (1)$$

where I is the identity matrix and **F** the deformation gradient. Linear approximation was chosen for **F** and evaluated via maximum likelihood estimation (Geers et al., 1996). Radius of the overlapping strain windows (representing the neighbourhood used to evaluate a single strain value at a specific voxel) was set to match the B-spline spacing after optimisation. The maximum compressive (that is, minimum principal) and maximum shear (γ_{max}, that is, absolute difference between maximum and minimum principal) strains were extracted (Oomens et al., 2003; Beer et al., 2009). Both have been proposed as potential indicators of tissue damage (Ceelen et al., 2008). Spatial variation of these quantities was evaluated in each subject along a critical path originating at the IT (most common site of pressure injuries Al-Dirini et al., 2017; Then et al., 2007; Makhsous et al., 2008) and pointing vertically towards the seat interface (Linder-Ganz et al., 2007; Oomens et al., 2003). To allow for direct comparison, the obtained curves were then interpolated to a common anatomy (subject 1) and the inter-subject average and standard deviation of the spatial variation of γ_{max} calculated.

It is important to note that results are presented in the scanner coordinate system, which is illustrated in Fig. 1a, alongside the direction of positive increment (that is, right-left (R→L), posterior-anterior (P→A) and inferior-superior (I→S)). These were selected to avoid ambiguity in interpreting anatomical coordinates for the semi-recumbent position.

3. Results

3.1. Initial global registration

Fig. 2 shows the results of the global registration on all the subjects analysed, using the optimal parameter set. The Dice coefficient showed subject mean of 80% in the alignment of the pelvic elements between partial-WB and full-WB, and 79% between non-WB and full-WB scans.

3.2. Displacement analysis

Patterns of displacement in Figs. 3 and 4 and average values in Fig. 5 showed an overall larger displacement at ROIs below the IT (medial ROIs) than below the GT (lateral ROIs), in both stages of deformation. The most prominent component of displacement was the P→A one, in particular in the 1st stage of deformation (non-WB to partial-WB). Alongside this vertical displacement, measurements showed simultaneous significant lateral components, that is, R→L and I→S. Although variable in magnitude across participants and ROIs, relatively large inferior displacements were measured, sometimes exceeding the P→A component, in particular in superficial ROIs. This was seen in both stages of deformation. The fat layer displaced inferiorly by 12.27 mm and 10.73 mm in the 1st and 2nd stages of deformation, respectively. Similarly, muscle displaced towards the inferior direction by an average of 5.81 mm and 7.93 mm, for the 1st and 2nd stages of deformation, respectively.

3.3. Strain analysis

Figs. 6 and 7 show the distribution of compressive strains for the overall transition from non-WB to full-WB. Polar plots of the strain components (Fig. 8) show an overall higher compression of the tissues in the 1st than in the 2nd stage of deformation. Interestingly, compression state of the deep muscle closer to the GT was generally higher (−8% in the 1st and −6% in the 2nd stage) than the compression just below the IT (−1% and −2%, respectively). The displacement of the gluteus maximus previously identified was not associated with any compression along the I→S direction, appearing as a prevalent shift of the tissue, facilitated by the ischial bursa which allows the muscle to slide relative to the bone.

The average spatial variation of maximum compressive and shear strains showed higher values closer to the seating interface than closer to the IT (Fig. 9). Maximum compressive strain was overall higher in the fat. However, when looking at the stages of deformation, fat compressed more than the muscle in the 1st stage of deformation, whereas in the 2nd stage, more compression occurred in the muscle. The maximum shear strain for the overall deformation peaked close to the interface with the muscle, reaching values just below 1. The peak was followed by a plateau in the centre of the muscle first, and then by a decrease towards the IT. Maximum shear strains were slightly higher on average in the 1st stage of deformation than in the 2nd, with the peak located in the deep muscle.

4. Discussion

The aim of the study was to measure the full-field, 3D, progressive deformation of the buttock due to sitting using DVC, relying on minimal *a priori* assumptions on the obtained deformation field. The study found, in line with the literature, that *in vivo* soft tissue deformation was larger near the IT than near the GT in both stages of deformation (Al-Dirini et al., 2017; Then et al., 2007; Makhsous et al., 2008). Most of the compressive P→A component occurred during the 1st stage of deformation (non-WB to partial-WB), with little to no further compression seen in the 2nd stage of deformation. Despite differences in magnitude, this overall deformation pattern was observed in almost all subjects in this study. Alongside this component, fat and superficial muscle tissues displaced away from the IT, predominantly in the inferior direction.

The captured shift of the superficial muscle below both the IT and GT confirmed and quantified (total average of 13.74 mm) the lateral sliding of the gluteal muscle tissue that was only qualitatively reported in the literature (Sonenblum et al., 2013; Doridam et al., 2018; Brienza et al., 2018; Wang et al., 2022). This shift is thought to leave little muscle below the IT bearing the sitting load, with the fat, ligaments and tendons withstanding the weight instead (Sonenblum et al., 2015; Doridam et al., 2018; Sonenblum et al., 2020). However, the muscle did not slide completely off the IT in the present study due to the semi-recumbent posture imaged (Sonenblum et al., 2020; Doridam et al., 2018): this result suggests that semi-recumbent and lying positions might be preferable over a sitting one to redistribute the load over a thicker layer of tissues (Linder-Ganz et al., 2008). The complexity of the deformation evaluated in the present study showed and highlighted the error committed by simplified FE models that disregard lateral deformation, representing only a small section of the buttocks, or missing an adequate representation of the bursae and the sliding between tissues (Sonenblum et al., 2020; Al-Dirini et al., 2016).

Although comparison is limited by methodological differences, acquired values of γ_{max} fell within values cited in the literature related to sitting and lying: Doridam et al. (2018) reported average shear strain above 0.75 from ultrasound-based DIC of 7 healthy subjects sitting on a stool. Similarly, Linder-Ganz et al. (2008) reported average γ_{max} strain from a FE simulation of around 0.90 in the fat and 0.41 in the muscle for healthy participants when sitting. Finally, the MR-validated FE simulation designed by Oomens et al. (2013) of healthy subjects lying on a hard spine board generated values up to 0.8. In the present study, regions showed similar progression of deformation between stages, with average γ_{max} of 0.44 ± 0.08 for the overall deformation (non-WB to full-WB condition). Only the fat and superficial muscle below the IT showed slightly higher γ_{max} in the 1st than in the 2nd stage.

Values of shear strain in the present study were calculated from a cohort of healthy participants in 1 h time window, with around 11 mins spent in each position (Al-Dirini et al., 2017). No incidence of pressure injury was reported. Nevertheless, alongside other works on human subjects (Doridam et al., 2018; Oomens et al., 2013; Linder-Ganz et al.,

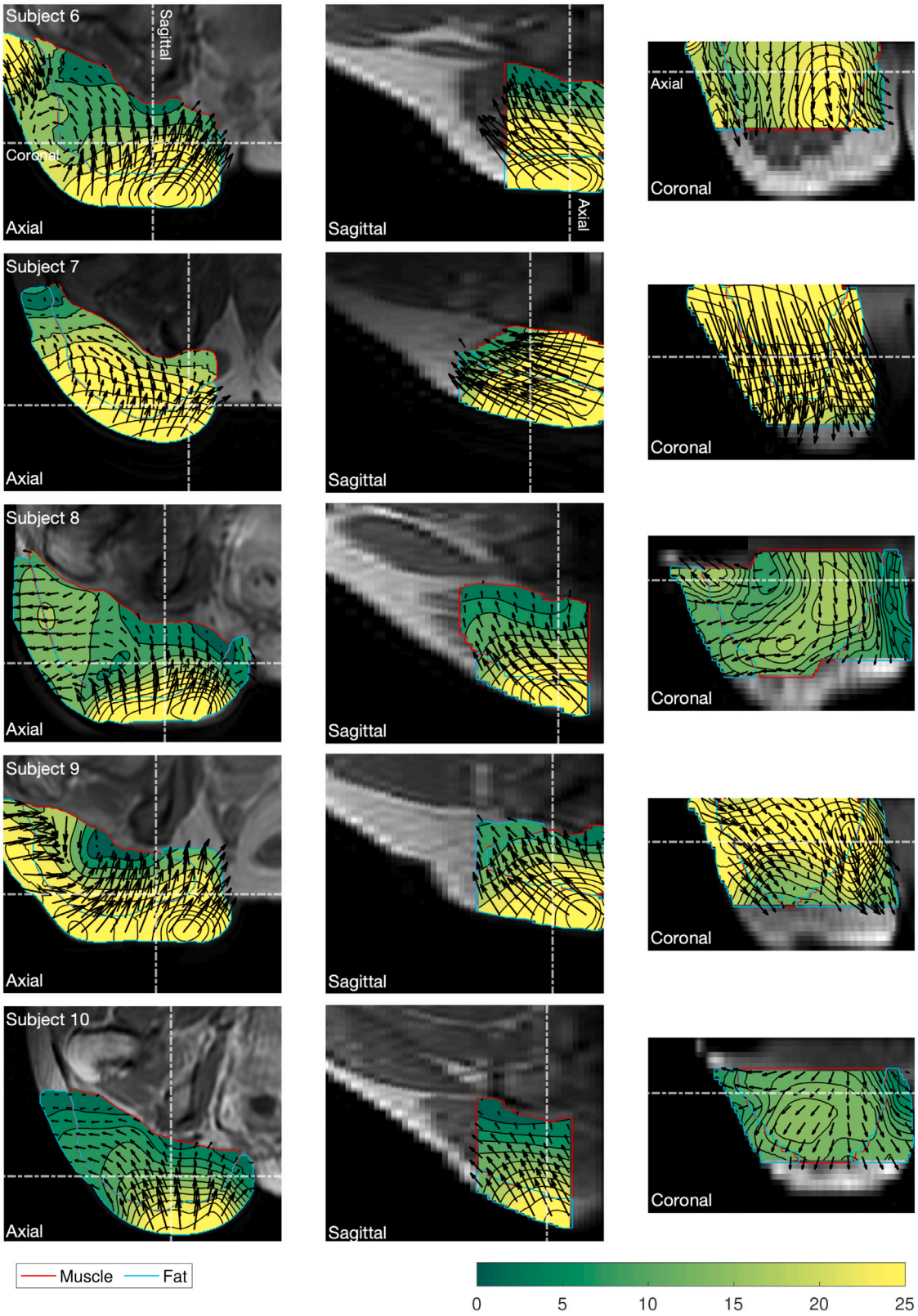

Fig. 4. Axial (left), sagittal (centre) and coronal (right) views of the displacement field for the last 5 subjects. Arrows show the direction of displacement vectors for the overall deformation (non-WB to full-WB). Length of vectors is scaled for visualisation purposes: magnitude is represented by the underlying colourmap (in [mm]). Muscle and fat ROIs are delineated in red and turquoise, respectively. Slices are located at the centre of the IT: dashed lines show the location of the other slices. (For interpretation of the references to colour in this figure legend, the reader is referred to the web version of this article.)

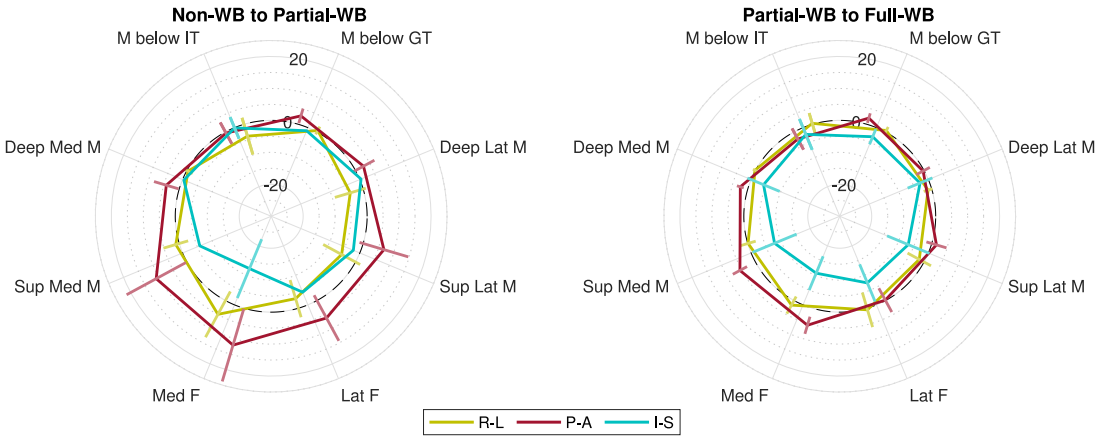

Fig. 5. Polar plots of the main components of the displacement field (in [mm], right-left (R→L), posterior-anterior (P→A) and inferior-superior (I→S)) for the two stages of deformation analysed. Values at the 1st stage of deformation (transition from non-WB to partial-WB) are reported on the left, whereas at the 2nd stage (from partial- to full-WB) is shown on the right. Statistics were evaluated over the following ROIs: Medial Fat, Superficial Medial Muscle, Deep Medial Muscle, Muscle below IT, Muscle below GT, Deep Lateral Muscle, Superficial Lateral Muscle, Lateral Fat. Bars represent inter-subject variability of mean regional values. Dashed circles depict the reference for zero displacement.

2008), the obtained values at IT exceeded the proposed thresholds of 0.45 max compressive strain and 0.75 γ_{max} for deformation-induced tissue injury based on mechanical indentation of the tibialis-anterior of a rat model up to 2 h (Ceelen et al., 2008), as well as the 0.5 max compressive strain for up to 1 h (Gefen et al., 2008). The results of the present work further support the need for a systematic investigation of the relationship between time of exposure and threshold value.

The spatial variation of γ_{max} on the critical path from the sitting interface to the IT confirmed the trend predicted by the FE simulation of Oomens et al. (2003), showing an initial peak at the fat layer, followed by a plateau in the muscle layer, and then a decrease of values towards the IT. Different to Oomens et al. (2003), peak values in this study were almost double those generated by their FE simulation and located closer to the muscle-fat interface. The spatial evolution of the compressive strain was found to be opposite to the one calculated via FE simulation in Linder-Ganz et al. (2007). Their trend showed a peak at the IT and a gradual decrease of values towards the seating interface. This difference could partially be related to both the extension of the simulated section of the buttock and the choice of boundary conditions between tissues. The results of the study draw attention on the importance of out-of-place displacements and boundary conditions on strain estimations.

The variability in the patterns of deformation that was captured in this study can be associated to the repeatability of the measurements as well as to inter- and intra-subject differences in tissue response. First, the parametric optimisation detailed in the Supplementary Materials was aimed at minimising the first source of uncertainty. Two simulated fields with biomechanically accurate characteristics were generated to identify the optimal parameter set, giving an error of 11% of the said fields. Second, the study cohort showed differences between subjects in terms of anthropometry and tissue response to load (Al-Dirini et al., 2017). Subjects 1 and 5 dropped the left side of the hips after boards were removed, leading to different directions of gravity between scans; subjects 3, 6 and 9 touched the seat in the non-WB position, resulting in residual load on the left buttock; subject 8 showed fat infiltration (Al-Dirini et al., 2017), which might have affected the overall mechanical response of the surrounding tissue (Sopher et al., 2011). Moreover, the population sample was characterised by diverse BMI values, partly explaining the anatomical differences between subjects found in the estimated fields. In addition, small adjustments in the distribution of tissues within the same body posture may have contributed to the variability in the results, as a mechanism for healthy subjects to avoid pressure injuries when sitting for long periods. The latter considerations illustrate the challenge in designing body supports such as seats and mattresses, that comfortably fit everyone as well as the individual. It is therefore critical that future studies consider each of these sources of variability in their design, with a more extensive subject recruitment and an improved repeatability of experimental set-up (Loerakker et al., 2011).

Finally, the semi-recumbent position chosen for the scanning had the limitation that the pelvis was located at opening of the scanner bore. MR distortions are known to affect scans by introducing a spurious spatial warping, which magnitude increases further away from the isocentre (Neumann et al., 2015; Watanabe et al., 2006; Dammann et al., 2011; Duchin et al., 2012): studies on 1.5T scanners reported distortions after correction below 2 mm (Karger et al., 2006; Tavares et al., 2014; Neumann et al., 2015). MR distortions were evident in slices near the superior pubic rami, even after the scanner-default distortion correction. Although limited in comparison to the magnitude of the deformation acquired in the present study, the spurious warping effect of MR distortions on the imaged anatomy needs further investigation, as it adds an additional component of error to the DVC measurements (Neumann et al., 2015).

5. Conclusion

The present study provides full-field, 3D, DVC measurements of soft tissue deformation in the buttock due to semi-recumbent sitting loads. This offers valuable new insights into the mechanics of pressure injury; measuring strains directly has significant advantages over finite element simulations as no assumptions about tissue properties or boundary conditions are made. A significant effort was made to minimise the error associated to the DVC calculations. Global registration of skeletal elements gave acceptable values of Dice coefficient around 80%, whereas the deformable registration showed an error of 0.99 mm against a simulated field replicating the transition from partial-WB to full-WB and 1.78 mm against a larger one simulating the non-to-partial-WB transition. The study depicted the complexity of the deformation and drew attention on the importance of isolating experimental factors affecting the response of tissues in future studies. On a global scale, the analysis of deformation permitted the quantification of the lateral slide of the gluteus maximus reported in the literature, and the role of the ischial bursa in facilitating its sliding: the muscle displaced inferiorly by about 6 mm in 1st stage, whereas by about 8 mm in the 2nd stage of deformation. The fat followed in a similar way, showing a shift of about 12 mm and 11 mm in the 1st and 2nd stage of deformation, respectively. On a local scale, the study allowed to measure the evolution of maximum compressive and γ_{max} along a path from the skin to the IT. Values peaked in the fat, close to the interface with the muscle, with values exceeding the damage thresholds of 0.45 max compressive strain

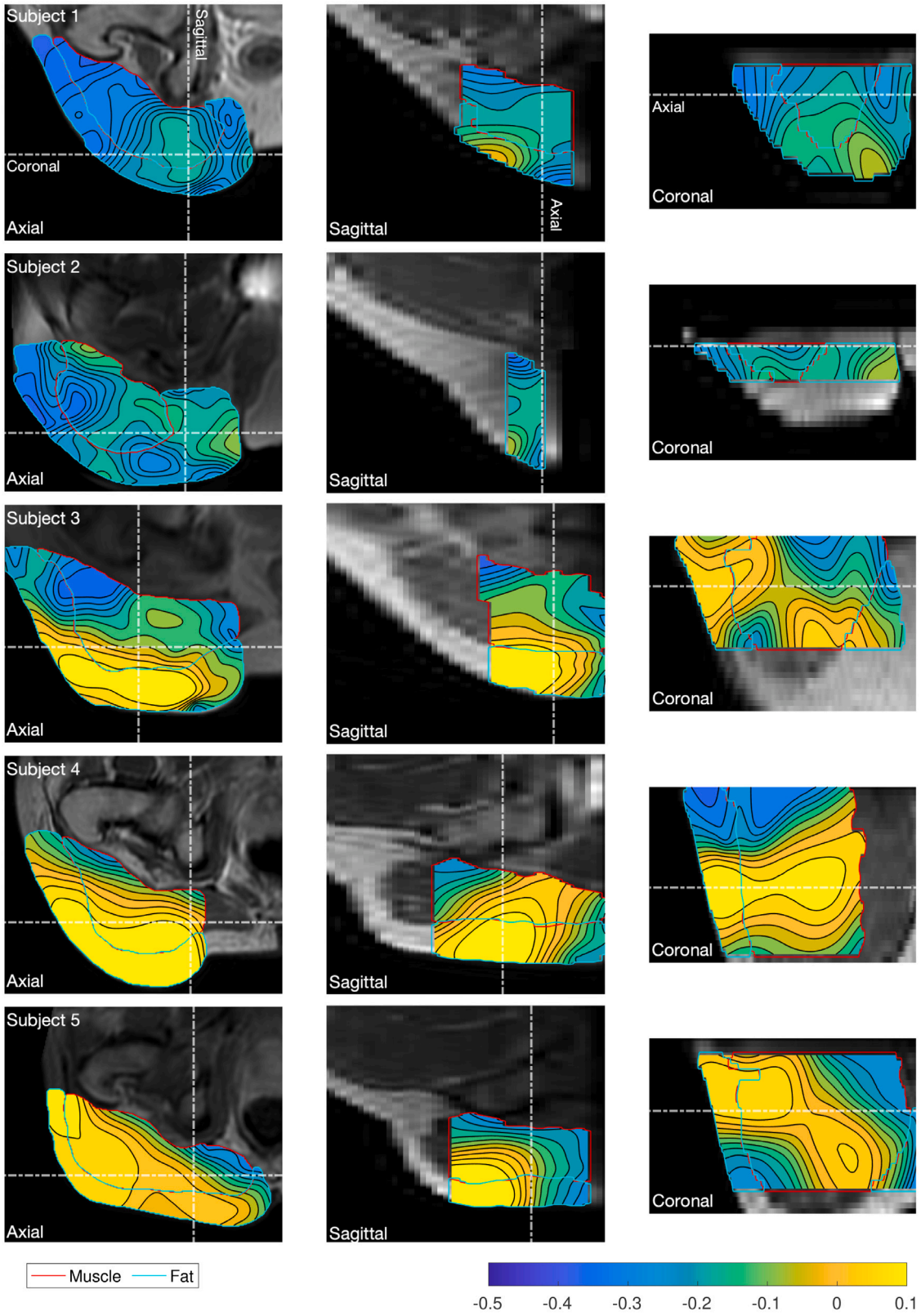

Fig. 6. Axial (left), sagittal (centre) and coronal (right) views of the distribution of the maximum compressive strain for the first 5 subjects. Values refer to the overall deformation (non-WB to full-WB). Muscle and fat ROIs are delineated in red and turquoise, respectively. Slices are located at the centre of the IT: dashed lines show the location of the other slices. (For interpretation of the references to colour in this figure legend, the reader is referred to the web version of this article.)

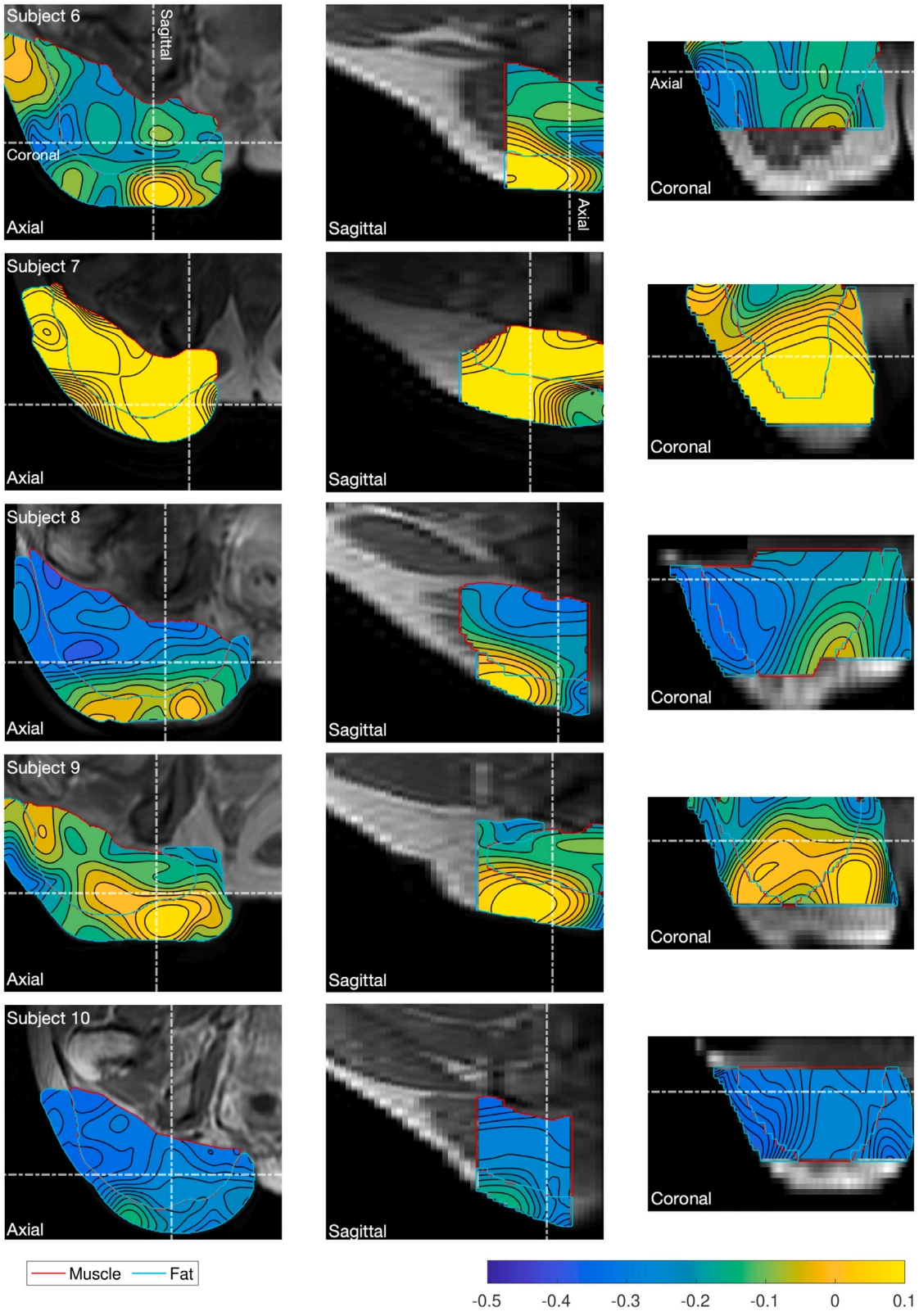

Fig. 7. Axial (left), sagittal (centre) and coronal (right) views of the distribution of the maximum compressive strain for the last 5 subjects. Values refer to the overall deformation (non-WB to full-WB). Muscle and fat ROIs are delineated in red and turquoise, respectively. Slices are located at the centre of the IT: dashed lines show the location of the other slices. (For interpretation of the references to colour in this figure legend, the reader is referred to the web version of this article.)

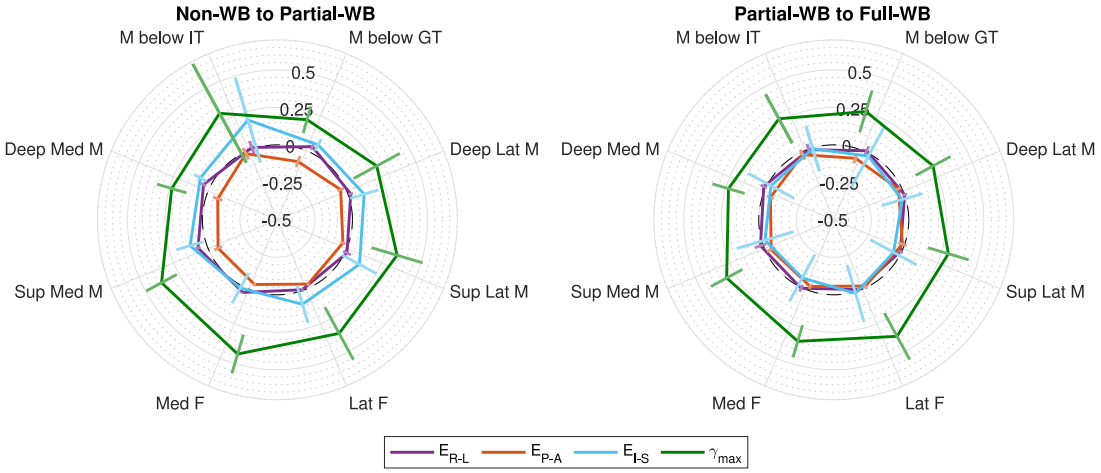

Fig. 8. Polar plots of the main components of the Lagrangian strain tensor ($E_{R\to L}$, $E_{P\to A}$, $E_{I\to S}$) and the maximum shear strain (γ_{max}). Values at the 1st stage of deformation (transition from non-WB to partial-WB) are reported on the left, whereas at the 2nd stage (from partial- to full-WB) is shown on the right. Statistics were evaluated over the following ROIs: Medial Fat, Superficial Medial Muscle, Deep Medial Muscle, Muscle below IT, Muscle below GT, Deep Lateral Muscle, Superficial Lateral Muscle, Lateral Fat. Bars represent inter-subject variability of mean regional values. Dashed circles depict the reference for zero strain.

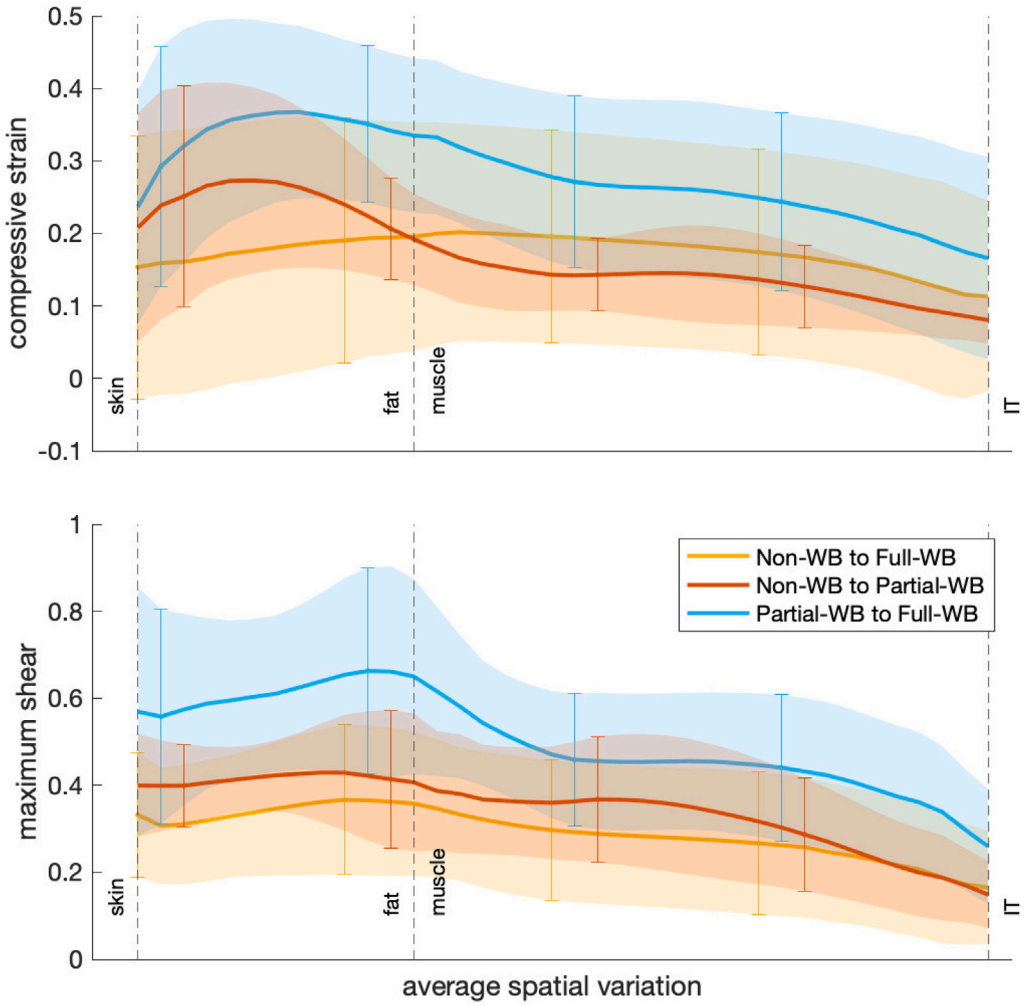

Fig. 9. Spatial variations of compressive strain (top) and maximum shear strain (bottom). Curves are reported for the overall deformation (yellow, non-WB to full-WB), for the 1st stage of deformation (orange, non-WB to partial-WB) and for the 2nd stage of deformation (blue, partial-WB to full-WB conditions). Lines represent average values between subjects, whereas shaded areas the variability in subject mean. (For interpretation of the references to colour in this figure legend, the reader is referred to the web version of this article.)

and 0.75 γ_{max} proposed in literature from rat model. The extensive measurements taken from this study will hopefully be beneficial in the further understanding of such complex deformation, and ultimately in the improvement of the design of control and prevention systems for DTIs.

CRediT authorship contribution statement

Stefano Zappalá: Writing – original draft, Visualization, Validation, Software, Resources, Project administration, Methodology, Investigation, Formal analysis, Data curation, Conceptualization. **Bethany E. Keenan:** Writing – review & editing, Supervision, Resources, Project administration, Methodology, Data curation, Conceptualization. **David Marshall:** Writing – review & editing, Supervision, Project administration, Conceptualization. **Jing Wu:** Writing – review & editing, Supervision, Conceptualization. **Sam L. Evans:** Writing – review & editing, Supervision, Project administration, Conceptualization. **Rami M.A. Al-Dirini:** Writing – review & editing, Supervision, Project administration, Data curation, Conceptualization.

Declaration of competing interest

The authors declare the following financial interests/personal relationships which may be considered as potential competing interests: Stefano Zappala reports a relationship with Neuralink Co that includes: consulting or advisory. Corresponding author published the work described in the manuscript in his doctoral thesis (8th Dec 2022), in line with the Elsevier policies.

Data availability

The dataset generated during and/or analysed during the current study are available in the following OSF repository (https://tinyurl.com/36x2npyt).

Acknowledgments

The research carried out did not received any external funding.

Appendix A. Supplementary data

Supplementary material related to this article can be found online at https://doi.org/10.1016/j.jbiomech.2023.111913.

References

Al-Dirini, R.M., Nisyrios, J., Reed, M.P., Thewlis, D., 2017. Quantifying the in vivo quasi-static response to loading of sub-dermal tissues in the human buttock using magnetic resonance imaging. Clin. Biomech. (ISSN: 18791271) 50 (September), 70–77. http://dx.doi.org/10.1016/j.clinbiomech.2017.09.017.

Al-Dirini, R.M., Reed, M.P., Hu, J., Thewlis, D., 2016. Development and validation of a high anatomical fidelity FE model for the buttock and thigh of a seated individual. Ann. Biomed. Eng. (ISSN: 15739686) 44 (9), 2805–2816. http://dx.doi.org/10.1007/s10439-016-1560-3.

Al-Dirini, R.M., Reed, M.P., Thewlis, D., 2015. Deformation of the gluteal soft tissues during sitting. Clin. Biomech. (ISSN: 18791271) 30 (7), 662–668. http://dx.doi.org/10.1016/j.clinbiomech.2015.05.008.

Avants, B.B., Epstein, C.L., Grossman, M., Gee, J.C., 2008. Symmetric diffeomorphic image registration with cross-correlation: Evaluating automated labeling of elderly and neurodegenerative brain. Med. Image Anal. (ISSN: 13618415) 12 (1), 26–41. http://dx.doi.org/10.1016/j.media.2007.06.004.

Avants, B.B., Tustison, N.J., Song, G., 2009. Advanced normalization tools (ANTS). Insight J. (ISSN: 09255273) 1–35.

Avril, S., Evans, S., Miller, K., 2013. Inverse problems and material identification in tissue biomechanics. J. Mech. Behav. Biomed. Mater. (ISSN: 17516161) 27, 129–131. http://dx.doi.org/10.1016/j.jmbbm.2013.07.001.

Bartley, C., Stephens, M., 2019. Development of Pressure Ulcers When Sitting, Vol. 15. Wounds UK, (ISSN: 17466814) pp. 34–39. http://dx.doi.org/10.17866/rd.salford.7958873, (1).

Beer, F.P., Johnston, E.R., DeWolf, J.T., Mazurek, D.F., 2009. Mechanics of Materials, fifth ed. McGraw-Hill Higher Education, New York, ISBN: 9780071284226.

Black, J.M., Brindle, C.T., Honaker, J.S., 2016. Differential diagnosis of suspected deep tissue injury. Int. Wound J. (ISSN: 1742481X) 13 (4), 531–539. http://dx.doi.org/10.1111/iwj.12471.

Bouten, C.V., Oomens, C.W., Baaijens, F.P., Bader, D.L., 2003. The etiology of pressure ulcers: Skin deep or muscle bound? Arch. Phys. Med. Rehabil. (ISSN: 00039993) 84 (4), 616–619. http://dx.doi.org/10.1053/apmr.2003.50038.

Brienza, D., Vallely, J., Karg, P., Akins, J., Gefen, A., 2018. An MRI investigation of the effects of user anatomy and wheelchair cushion type on tissue deformation. J. Tissue Viability (ISSN: 18764746) 27 (1), 42–53. http://dx.doi.org/10.1016/j.jtv.2017.04.001.

Bucki, M., Luboz, V., Perrier, A., Cannard, F., Diot, B., Vuillerme, N., Payan, Y., 2019. Body Numerical Phantoms for Estimating Soft Tissue Pains or Injuries When Interacting with Shoes, Seats and Mattresses. HAL, archives-ouvertes.fr.

Ceelen, K.K., Stekelenburg, A., Loerakker, S., Strijkers, G.J., Bader, D.L., Nicolay, K., Baaijens, F.P., Oomens, C.W., 2008. Compression-induced damage and internal tissue strains are related. J. Biomech. (ISSN: 00219290) 41 (16), 3399–3404. http://dx.doi.org/10.1016/j.jbiomech.2008.09.016.

Chen, S., Scott, J., Bush, T.R., Roccabianca, S., 2020. Inverse finite element characterization of the human thigh soft tissue in the seated position. Biomech. Model. Mechanobiol. (ISSN: 16177940) 19 (1), 305–316. http://dx.doi.org/10.1007/s10237-019-01212-7.

Dammann, P., Kraff, O., Wrede, K.H., Özkan, N., Orzada, S., Mueller, O.M., Sandalcioglu, I.E., Sure, U., Gizewski, E.R., Ladd, M.E., Gasser, T., 2011. Evaluation of hardware-related geometrical distortion in structural MRI at 7 tesla for image-guided applications in neurosurgery. Academic Radiol. (ISSN: 10766332) 18 (7), 910–916. http://dx.doi.org/10.1016/j.acra.2011.02.011.

Dice, L.R., 1945. Measures of the amount of ecologic association between species. Ecology (ISSN: 0012-9658) 26 (3), 297–302. http://dx.doi.org/10.2307/1932409.

Doridam, J., Macron, A., Vergari, C., Verney, A., Rohan, P.Y., Pillet, H., 2018. Feasibility of sub-dermal soft tissue deformation assessment using B-mode ultrasound for pressure ulcer prevention. J. Tissue Viability (ISSN: 18764746) 27 (4), 238–243. http://dx.doi.org/10.1016/j.jtv.2018.08.002.

Duchin, Y., Abosch, A., Yacoub, E., Sapiro, G., Harel, N., 2012. Feasibility of using ultra-high field (7 T) MRI for clinical surgical targeting. PLoS ONE (ISSN: 19326203) 7 (5), 1–10. http://dx.doi.org/10.1371/journal.pone.0037328.

Ebner, M., Wang, G., Li, W., Aertsen, M., Patel, P.A., Aughwane, R., Melbourne, A., Doel, T., Dymarkowski, S., De Coppi, P., David, A.L., Deprest, J., Ourselin, S., Vercauteren, T., 2020. An automated framework for localization, segmentation and super-resolution reconstruction of fetal brain MRI. NeuroImage (ISSN: 10959572) 206 (September 2019), http://dx.doi.org/10.1016/j.neuroimage.2019.116324.

Fletcher, J., Bader, D., Downie, F., Dowsett, C., Milne, J., Ousey, K., Schoonhoven, L., 2017. Recognising, Managing and Preventing Deep Tissue Injury (DTI). Tech. Rep..

Fletcher, J., Crook, H., Harris, C., 2013. Monitoring Pressure Ulcer Prevalence: A Precise Methodology, Vol. 9. Wounds UK, (ISSN: 17466814) pp. 48–53, (4).

Geers, M.G., De Borst, R., Brekelmans, W.A., 1996. Computing strain fields from discrete displacement fields in 2d-solids. Int. J. Solids Struct. (ISSN: 00207683) http://dx.doi.org/10.1016/0020-7683(95)00240-5.

Gefen, A., 2008. How much time does it take to get a pressure ulcer? Integrated evidence from human, animal, and in vitro studies. Ostomy Wound Manag. (ISSN: 08895899) 54 (10).

Gefen, A., Van Nierop, B., Bader, D.L., Oomens, C.W., 2008. Strain-time cell-death threshold for skeletal muscle in a tissue-engineered model system for deep tissue injury. J. Biomech. (ISSN: 00219290) 41 (9), 2003–2012. http://dx.doi.org/10.1016/j.jbiomech.2008.03.039.

Guest, J.F., Fuller, G.W., Vowden, P., 2020. Cohort study evaluating the burden of wounds to the UK's National Health Service in 2017/2018: Update from 2012/2013. BMJ Open (ISSN: 20446055) 10 (12), 1–15. http://dx.doi.org/10.1136/bmjopen-2020-045253.

Holzapfel, G., 2002. Nonlinear solid mechanics: A continuum approach for engineering science. http://dx.doi.org/10.1023/A:1020843529530.

Jenkinson, M., Bannister, P., Brady, M., Smith, S., 2002. Improved optimization for the robust and accurate linear registration and motion correction of brain images. NeuroImage (ISSN: 10538119) 17 (2), 825–841. http://dx.doi.org/10.1006/nimg.2002.1132.

Karger, C.P., Höss, A., Bendl, R., Canda, V., Schad, L., 2006. Accuracy of device-specific 2D and 3D image distortion correction algorithms for magnetic resonance imaging of the head provided by a manufacturer. Phys. Med. Biol. (ISSN: 00319155) 51 (12), N253–61. http://dx.doi.org/10.1088/0031-9155/51/12/N04.

Klein, S., Staring, M., 2011. elastix: The manual. In: October, Vol. 2011. pp. 1–42, (6).

Klein, S., Staring, M., Murphy, K., Viergever, M.A., Pluim, J.P., 2010. Elastix: A toolbox for intensity-based medical image registration. IEEE Trans. Med. Imaging (ISSN: 02780062) 29 (1), 196–205. http://dx.doi.org/10.1109/TMI.2009.2035616.

Linder-Ganz, E., Shabshin, N., Itzchak, Y., Gefen, A., 2007. Assessment of mechanical conditions in sub-dermal tissues during sitting: A combined experimental-MRI and finite element approach. J. Biomech. (ISSN: 00219290) 40 (7), 1443–1454. http://dx.doi.org/10.1016/j.jbiomech.2006.06.020.

Linder-Ganz, E., Shabshin, N., Itzchak, Y., Yizhar, Z., Siev-Ner, I., Gefen, A., 2008. Strains and stresses in sub-dermal tissues of the buttocks are greater in paraplegics than in healthy during sitting. J. Biomech. (ISSN: 00219290) 41 (3), 567–580. http://dx.doi.org/10.1016/j.jbiomech.2007.10.011.

Loerakker, S., Manders, E., Strijkers, G.J., Nicolay, K., Baaijens, F.P., Bader, D.L., Oomens, C.W., 2011. The effects of deformation, ischemia, and reperfusion on the development of muscle damage during prolonged loading. J. Appl. Physiol. (ISSN: 87507587) 111 (4), 1168–1177. http://dx.doi.org/10.1152/japplphysiol.00389.2011.

Maas, S.A., Ellis, B.J., Ateshian, G.A., Weiss, J.A., 2012. FEBio: Finite elements for biomechanics. J. Biomech. Eng. (ISSN: 01480731) 134, http://dx.doi.org/10.1115/1.4005694.

Macron, A., Pillet, H., Doridam, J., Rivals, I., Sadeghinia, M.J., Verney, A., Rohan, P.Y., 2020. Is a simplified Finite Element model of the gluteus region able to capture the mechanical response of the internal soft tissues under compression? Clin. Biomech. (ISSN: 18791271) 71 (October 2019), 92–100. http://dx.doi.org/10.1016/j.clinbiomech.2019.10.005.

Makhsous, M., Lin, F., Cichowski, A., Cheng, I., Fasanati, C., Grant, T., Hendrix, R.W., 2011. Use of MRI images to measure tissue thickness over the ischial tuberosity at different hip flexion. Clin. Anat. (ISSN: 08973806) 24 (5), 638–645. http://dx.doi.org/10.1002/ca.21119.

Makhsous, M., Venkatasubramanian, G., Chawla, A., Pathak, Y., Priebe, M., Rymer, W.Z., Lin, F., 2008. Investigation of soft-tissue stiffness alteration in denervated human tissue using an ultrasound indentation system. J. Spinal Cord Med. (ISSN: 10790268) 31 (1), 88–96. http://dx.doi.org/10.1080/10790268.2008.11753987.

Monea, A.G., Verpoest, I., Vander Sloten, J., Van Der Perre, G., Goffin, J., Depreitere, B., 2012. Assessment of relative brain-skull motion in quasistatic circumstances by magnetic resonance imaging. J. Neurotrauma (ISSN: 08977151) 29 (13), 2305–2317. http://dx.doi.org/10.1089/neu.2011.2271.

Nelissen, J.L., Traa, W.A., de Boer, H.H., De Graaf, L., Mazzoli, V., Savci-Heijink, C.D., Nicolay, K., Froeling, M., Bader, D.L., Nederveen, A.J., Oomens, C.W., Strijkers, G.J., 2018. An advanced magnetic resonance imaging perspective on the etiology of deep tissue injury. J. Appl. Physiol. (ISSN: 15221601) 124 (6), 1580–1596. http://dx.doi.org/10.1152/japplphysiol.00891.2017.

Neumann, J.O., Giese, H., Biller, A., Nagel, A.M., Kiening, K., 2015. Spatial distortion in MRI-guided stereotactic procedures: Evaluation in 1.5-, 3- and 7-tesla MRI scanners. Stereotact. Funct. Neurosurg. (ISSN: 14230372) 93 (6), 380–386. http://dx.doi.org/10.1159/000441233.

Oliveira, F.P.M., Tavares, J.M.R.S., 2014. Medical image registration: a review. Comput. Methods Biomech. Biomed. Eng. (ISSN: 1476-8259) 17 (10), 73–93. http://dx.doi.org/10.1080/10255842.2012.670855.

Oomens, C.W., Bressers, O.F., Bosboom, E.M., Bouten, C.V., Bader, D.L., 2003. Can loaded interface characteristics influence strain distributions in muscle adjacent to bony prominences? Comput. Methods Biomech. Biomed. Eng. (ISSN: 10255842) 6 (3), 171–180. http://dx.doi.org/10.1080/1025584031000121034.

Oomens, C.W., Zenhorst, W., Broek, M., Hemmes, B., Poeze, M., Brink, P.R., Bader, D.L., 2013. A numerical study to analyse the risk for pressure ulcer development on a spine board. Clin. Biomech. (ISSN: 02680033) 28 (7), 736–742. http://dx.doi.org/10.1016/j.clinbiomech.2013.07.005.

Ou, Y., Sotiras, A., Paragios, N., Davatzikos, C., 2011. DRAMMS: Deformable registration via attribute matching and mutual-saliency weighting. Med. Image Anal. (ISSN: 13618415) 15 (4), 622–639. http://dx.doi.org/10.1016/j.media.2010.07.002.

Schnabel, J.A., Tanner, C., Castellano-Smith, A.D., Degenhard, A., Leach, M.O., Hose, D.R., Hill, D.L., Hawkes, D.J., 2003. Validation of nonrigid image registration using finite-element methods: Application to breast MR images. IEEE Trans. Med. Imaging (ISSN: 02780062) 22 (2), 238–247. http://dx.doi.org/10.1109/TMI.2002.808367.

Schnaudigel, S., Preul, C., Ugur, T., Mentzel, H.J., Witte, O.W., Tittgemeyer, M., Hagemann, G., 2010. Positional brain deformation visualized with magnetic resonance morphometry. Neurosurgery (ISSN: 0148396X) 66 (2), 376–384. http://dx.doi.org/10.1227/01.NEU.0000363704.74450.B4.

Schwartz, D., Gefen, A., 2019. The biomechanical protective effects of a treatment dressing on the soft tissues surrounding a non-offloaded sacral pressure ulcer. Int. Wound J. (ISSN: 1742481X) 16 (3), 684–695. http://dx.doi.org/10.1111/iwj.13082.

Shabshin, N., Zoizner, G., Herman, A., Ougortsin, V., Gefen, A., 2010. Use of weight-bearing MRI for evaluating wheelchair cushions based on internal soft-tissue deformations under ischial tuberosities. J. Rehabil. Res. Dev. (ISSN: 07487711) 47, 31–42. http://dx.doi.org/10.1682/JRRD.2009.07.0105.

Sonenblum, S.E., Seol, D., Sprigle, S.H., Cathcart, J.M.K., 2020. Seated buttocks anatomy and its impact on biomechanical risk. J. Tissue Viability (ISSN: 18764746) 29 (2), 69–75. http://dx.doi.org/10.1016/j.jtv.2020.01.004.

Sonenblum, S.E., Sprigle, S.H., Cathcart, J.M.K., Winder, R.J., 2013. 3-dimensional buttocks response to sitting: A case report. J. Tissue Viability (ISSN: 0965206X) 22 (1), 12–18. http://dx.doi.org/10.1016/j.jtv.2012.11.001.

Sonenblum, S.E., Sprigle, S.H., Cathcart, J.M.K., Winder, R.J., 2015. 3D anatomy and deformation of the seated buttocks. J. Tissue Viability (ISSN: 18764746) 24 (2), 51–61. http://dx.doi.org/10.1016/j.jtv.2015.03.003.

Sopher, R., Nixon, J., Gorecki, C., Gefen, A., 2011. Effects of intramuscular fat infiltration, scarring, and spasticity on the risk for sitting-acquired deep tissue injury in spinal cord injury patients. J. Biomech. Eng. (ISSN: 01480731) 133 (2), http://dx.doi.org/10.1115/1.4003325.

Sotiras, A., Davatzikos, C., Paragios, N., 2013. Deformable medical image registration: A survey. IEEE Trans. Med. Imaging (ISSN: 02780062) 32 (7), 1153–1190. http://dx.doi.org/10.1109/TMI.2013.2265603.

Tavares, W.M., Tustumi, F., Da Costa Leite, C., Gamarra, L.F., Amaro, E., Teixeira, M.J., Fonoff, E.T., 2014. An image correction protocol to reduce distortion for 3-T stereotactic MRI. Neurosurgery (ISSN: 0148396X) 74 (1), 121–126. http://dx.doi.org/10.1227/NEU.0000000000000178.

Then, C., Menger, J., Benderoth, G., Alizadeh, M., Vogl, T.J., Hübner, F., Silber, G., 2007. A method for a mechanical characterisation of human gluteal tissue. Technol. Health Care (ISSN: 09287329) 15 (6), 385–398. http://dx.doi.org/10.3233/thc-2007-15601.

Wang, X., Savonnet, L., Duprey, S., 2022. A Preliminary Study on the Effects of Foam and Seat Pan Inclination on the Deformation of the Seated Buttocks Using MRI. In: LNNS, vol. 223, Springer Science and Business Media Deutschland GmbH, ISBN: 9783030746131, pp. 434–438. http://dx.doi.org/10.1007/978-3-030-74614-8_55.

Watanabe, Y., Lee, C.K., Gerbi, B.J., 2006. Geometrical accuracy of a 3-tesla magnetic resonance imaging unit in Gamma Knife surgery. J. Neurosurg. (ISSN: 00223085) 105 (Supplement), 190–193. http://dx.doi.org/10.3171/sup.2006.105.7.190.

Westby, M.J., Dumville, J.C., Soares, M.O., Stubbs, N., Norman, G., 2017. Dressings and topical agents for treating pressure ulcers. Cochrane Database Syst. Rev. (ISSN: 1469493X) 2017 (6), http://dx.doi.org/10.1002/14651858.CD011947.pub2.

Xu, Z., Lee, C.P., Heinrich, M.P., Modat, M., Rueckert, D., Ourselin, S., Abramson, R.G., Landman, B.A., 2016. Evaluation of six registration methods for the human abdomen on clinically acquired CT. IEEE Trans. Biomed. Eng. (ISSN: 15582531) 63 (8), 1563–1572. http://dx.doi.org/10.1109/TBME.2016.2574816.

Zappalá, S., Bennion, N.J., Potts, M.R., Wu, J., Kusmia, S., Jones, D.K., Evans, S.L., Marshall, D., 2021. Full-field MRI measurements of in-vivo positional brain shift reveal the significance of intra-cranial geometry and head orientation for stereotactic surgery. Sci. Rep. 11 (1), 17684. http://dx.doi.org/10.1038/S41598-021-97150-5.

Zeevi, T., Levy, A., Brauner, N., Gefen, A., 2018. Effects of ambient conditions on the risk of pressure injuries in bedridden patients—multi-physics modelling of microclimate. Int. Wound J. (ISSN: 1742481X) 15 (3), 402–416. http://dx.doi.org/10.1111/iwj.12877.